

Ab initio prediction of stable nanotwin double layers and 4O structure in Ni_2MnGa

Martin Zelený,^{1,2,3,*} Ladislav Straka,³ Alexei Sozinov,⁴ and Oleg Heczko³

¹*Institute of Materials Science and Engineering, NETME Centre,
Faculty of Mechanical Engineering, Brno University of Technology,
Technická 2896/2, CZ-616 69 Brno, Czech Republic*

²*Central European Institute of Technology, CEITEC MU,
Masaryk University, Kamenice 753/5, CZ-625 00 Brno, Czech Republic*

³*Institute of Physics, Academy of Sciences of the Czech Republic,
Na Slovance 1999/2, CZ-182 21 Prague, Czech Republic*

⁴*Material Physics Laboratory, Lappeenranta University of Technology, Laitaatsillantie 3, FI-57170 Savonlinna, Finland*
(Dated: January 6, 2017)

The *ab initio* electronic structure calculations of the Ni_2MnGa alloy indicate that the orthorhombic 4O structure exhibits the lowest energy compared to all known martensitic structures. The 4O structure is formed by nanotwin double layers, i.e., oppositely oriented nanotwins consisting of two (101) lattice planes of nonmodulated martensitic structure. It exhibits the lowest occupation of density of states at the Fermi level. The total energy 1.98 meV/atom below the energy of nonmodulated martensite is achieved within structural relaxation by shifting Mn and Ga atoms at the nanotwin boundaries. The same atomic shift can also be found in other martensitic nanotwinned or modulated structures such as 10M and 14M, which indicates the importance of the nanotwin double layer for the stability of these structures. Our discovery shows that the nanotwinning or modulation is a natural property of low-temperature martensitic phases in Ni-Mn-Ga alloys.

PACS numbers: 81.30.Kf, 71.15.Nc, 61.50.-f, 64.60.My

Among Heusler alloys, the Ni_2MnGa is one of the few, which exhibit the unique properties resulting in a giant magnetic field-induced strain (MFIS) in their low-temperature martensitic phase¹. The MFIS can reach up to 12 % in case of Co- and Cu-doped Ni_2MnGa ². Important factors enabling the MFIS are large magnetocrystalline anisotropy and extraordinarily high mobility of martensite twin boundaries^{3–6} that primarily depends on martensite structure. While at elevated temperature there is a single austenitic phase of Ni_2MnGa with cubic L2_1 structure, several low-temperature martensitic phases have been observed depending on composition, temperature and applied stress^{7–9}. Martensitic phases with orthorhombic or monoclinic structures exhibit modulation of (110) planes in $[\bar{1}\bar{1}0]$ direction with the periodicity of ten or fourteen lattice planes (10M or 14M). The third martensitic phase with nonmodulated (NM) tetragonally distorted L2_1 structure is typical for larger deviation from stoichiometry. In addition, above the martensitic transformation temperature there is a cubic premartensite with the periodicity of six lattice planes (6M) in alloys with small deviation from stoichiometry¹⁰.

Low-temperature instability of L2_1 austenite can be explained by a strong Fermi surface nesting responsible for the phonon softening in $[110]$ direction, which explains structural modulation of 6M premartensite^{11–14}. In addition there is also a large $\text{Ni-}e_g$ peak corresponding to antibonding states right below the Fermi level, E_f , in the minority density of states (DOS) channel. Due to the band Jahn-Teller effect the L2_1 cubic structure lowers its symmetry, which pushes the peak above E_f resulting in lower energy^{15–17}. Nonetheless, the precise causes of the variety of observed low temperature martensitic phases

and mechanism of intermartensitic transformations between them have not been fully explained yet.

Ab initio calculations have been employed to understand modulations in Ni_2MnGa . Early works used description of 10M and 14M martensite with the help of pseudo-tetragonal structures with harmonic modulation, but this approximation resulted in total energy approximately in the middle between energies of the austenite and NM structure^{18–21}. This is in conflict with apparent stable modulated structure observed for alloys close to stoichiometry at low temperatures^{22,23}.

Later, the modulated martensites have been described by monoclinic structures with an alternating sequence of nanotwins constituted from (101) lattice planes of NM structure shown in Fig. 1(a). The 14M (denoted as $(5\bar{2})_2$, Fig. 1(b)) comprises of five lattice planes in one orientation and two planes in the other orientation. This is repeated twice to fulfill the atomic ordering^{24–26}. Similarly the 10M structure can be considered as alternating nanotwins of width three and two lattice planes (denoted as $(3\bar{2})_2$, Fig. 1(c))²⁷. The nanotwin description is based on the theory of adaptive martensite²⁸, where modulated structures are derived from the accommodation of the geometrical mismatch at the interface between austenite and martensite²⁵. In contrast with harmonic modulation the fully relaxed $(3\bar{2})_2$ and $(5\bar{2})_2$ structures with zig-zag modulation give *ab initio* total energies very close to the total energy of NM structure within 0.7 meV/atom interval.

Yet, the succession of structures with decreasing total energy at 0 K depends on the calculation settings. The successions of 14M, 10M and NM structures²⁹, 10M, 14M and NM structures³⁰ and even 10M, NM and

14M structures³¹ have been reported in contrast to experiment where only 10M structure has been observed for stoichiometric single crystal¹⁶. For off-stoichiometry composition the (10M \rightarrow) 14M \rightarrow NM sequences of intermartensitic transformations occur with decreasing temperature^{32,33}. Recent *ab initio* calculations of the Ni₂MnGa phase diagram which include lattice and vibrational degrees of freedom propose that the stability of martensite and intermartensitic transformation can be understood solely using thermodynamic concepts³¹. However, such predictions for low-temperature part of phase diagram are still uncertain due to the small structural energy difference between martensitic phases.

The (3 $\bar{2}$)₂ and (5 $\bar{2}$)₂ structures can be conceptually transformed into the NM phase by reorientation of nanotwins constituted from two basal planes – nanotwin doublelayer³⁴ as shown in Fig. 1. The transformation can be viewed as application of local shear in (101) plane along the [10 $\bar{1}$] direction³⁵. The doublelayer nanotwin reorientation was indicated in recent experimental in-situ study of stress-induced 14M \rightarrow NM transformation using high resolution TEM³⁶. Transformation between (3 $\bar{2}$)₂ and (5 $\bar{2}$)₂ structures can be described similarly but mechanism is more complex, because it includes cooperative reorientation of several nanotwin doublelayers.

The shear-based transformation concept does not include motion of twinning dislocations observed in experiment, yet it shows the relevance of nanotwin doublelayer for the intermartensitic transformation and the stability of modulated structure. Gruner³⁷ conjectured that the structure based only on oppositely oriented double layers, denoted as 4O²⁶, might be even lower in energy by a few meV/f.u than other martensitic structures. Moreover the TEM reveals a very frequent stacking error of modulation in 14M structure, e. g. the sequence of (5 $\bar{2}$ 2 $\bar{2}$ 5)³⁶ containing three nanotwin doublelayers, which indicates the stability of doublelayer multistacks. The 4O structure has been suggested for Ni₅₀Mn₃₇Sb₁₃, Ni₅₀Mn_{37.5}Sn_{12.5} and Ni₅₀Mn₃₅In₁₅ to explain experimental diffraction patterns³⁸ but was never reported in Ni-Mn-Ga.

Thus, both theoretical concept and experiments indicate the importance of nanotwin doublelayers. This paper presents *ab initio* study of the 4O structure formed by nanotwin doublelayers, newly suggested in Ni₂MnGa alloy, and the comparison of its stability with respect to austenite and known martensitic structures.

Presented *ab initio* calculations were performed using the Vienna Ab-initio Simulation Package (VASP)^{39,40} in which the electron-ion interaction was described by projector-augmented wave potentials^{41,42}. The electronic orbitals were expanded in terms of plane waves with a maximum kinetic energy of 600 eV. We used the gradient-corrected exchange-correlation functional proposed by Perdew, Burke, and Ernzerhof⁴³. The Brillouin zone (BZ) was sampled using a Γ -point centered mesh with the smallest allowed spacing between k -points equal to 0.1 Å⁻¹ in each direction of the reciprocal lattice vectors. This setting ensured constant k -points density in

all our calculations. The integration over the BZ used the Methfessel-Paxton smearing method⁴⁴ with 0.02 eV smearing width. Settings for k -point density and smearing width were obtained with the help of adaptive smearing method⁴⁵. The total energy was calculated with a high precision by convergence to 10⁻⁷ eV per computational cell. Relaxation of the atomic positions and structural parameters were performed by the quasi-Newton algorithm, using the exact Hellmann-Feynman forces, and was considered to be converged after all forces dropped below 1 meV/Å⁻¹.

The calculated total energies for different structures are shown in Fig. 2(e). The differences between the austenite and martensitic structures are 4.48 meV/atom for 10M martensite described by fully relaxed (3 $\bar{2}$)₂ structure, 4.54 meV/atom for NM martensite, and 4.92 meV/atom for 14M martensite described by fully relaxed (5 $\bar{2}$)₂ structure. These results are in good agreement with the previous investigations³¹ although in some studies the NM martensite exhibits slightly lower energy than 14M^{29,30}. In addition to the previously reported martensitic phases, we have found the 4O martensitic structure as displayed in Fig. 1(e), which exhibits significantly lower total energy about 6.52 meV/atom below the total energy of the austenite.

The 4O structure in Fig. 1(e) constitutes from alternating doublelayer nanotwins and thus can be denoted as (22)₁. The subscript indicates that the sequence is repeated only once. In comparison to the ordinary NM structure with $(c/a)_{\text{NM}} = 1.250$ determined by *ab initio* calculations¹¹, the energy of 4O is 1.98 meV/atom lower (see Fig. 2(e)). Thus, our calculation indicates that neither previously described modulated nor NM structures are the true ground state of stoichiometric Ni₂MnGa alloy at 0 K.

The primitive cell of the 4O structure contains 16 atoms and exhibits simple orthorhombic symmetry with $(c/a)_{4\text{O}} = 1.97$, $(b/a)_{4\text{O}} = 1.27$ and lattice constant $a = 4.279$ Å. These 16 atoms form two nanotwin doublelayers, which are constituted from tetragonal building blocks with internal ratio $(c/a)_{\text{int}} \approx 1.20$. This ratio is different from NM, 10M or 14M structures³⁰ with $(c/a)_{\text{int}} = 1.25$. Creation of alternating nanotwins doublelayers from $(c/a)_{\text{int}} = 1.25$ blocks, which was starting atomic configuration before relaxation (see Fig. 2(a)), leads to total energy 1.00 meV/atom above the NM structure (see Fig. 2(e)). The lattice parameters of this ideal structure were obtained from geometrical considerations²⁶ using the equations:

$$a_{4\text{O}} = a_{\text{int}} \sqrt{1 + \left(\frac{c}{a}\right)_{\text{int}}^2}, b_{4\text{O}} = 2a_{\text{int}}, c_{4\text{O}} = \frac{4a_{\text{int}}^2 \left(\frac{c}{a}\right)_{\text{int}}}{a_{4\text{O}}}, \quad (1)$$

where $(c/a)_{\text{int}} = (c/a)_{\text{NM}}$ and $a_{\text{int}} = a_{\text{NM}}/2$. Atomic volume was kept constant and equal to the equilibrium NM structure volume.

The ideal 4O structure is not stable and thus will relax to the above described ground state. This was achieved

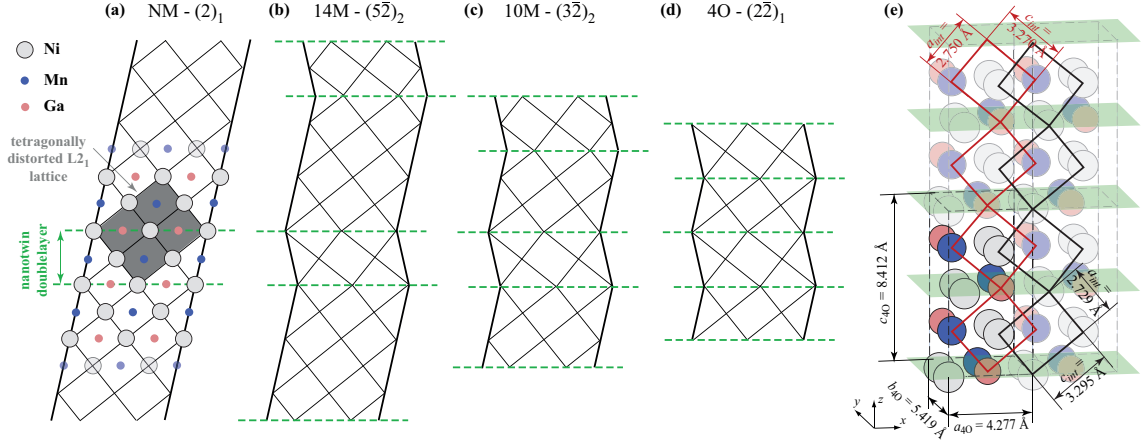


FIG. 1: (Color online) Schematic view of (a) NM, (b) 14M, (c) 10M, and (d) studied 4O structure. The thin black lines mark tetragonal building blocks. One of the NM cells with tetragonally distorted $L2_1$ structure, consisting of eight tetragonal building blocks (only four visible), is exemplarily marked in gray. The green dashed lines mark doublelayer nanotwin boundaries constituted from (101) lattice planes of NM structure. (e) Detail description of calculated 4O structure ($2 \times 1 \times 2$ supercell displayed with highlighted unit cell) with lattice parameters a_{4O} , b_{4O} and c_{4O} , and internal dimensions c_{int} and a_{int} of its tetragonal building blocks in Ni sublattices (black rectangles) and Mn-Ga sublattices (red rectangles). Green planes indicate nanotwin boundaries in (101) planes of NM structure.

by full unconstrained relaxation of lattice parameters and atomic positions based on Hellmann-Feynman forces. However, for the purpose of pointing out the most important lattice changes responsible for stabilization of structure, we intentionally divided the relaxation process into several steps. During each step, only selected parameters or positions were allowed to change while remaining ones were artificially constrained. Both unconstrained and constrained approaches resulted in the same equilibrium structure.

In the first relaxation step, decreasing $(c/a)_{int}$ of the tetragonal blocks to value 1.205 at the constant cell volume (Fig. 2(b)) decreased the total energy to the level 0.32 meV/atom below the NM structure, but still above the 14M structure. The relaxation of lattice parameters accompanied by modest volume expansion (Fig. 2(c)) further decreased the total energy to the level 0.72 meV/atom below the NM structure.

The essential decrease of the total energy by additional 1.26 meV/atom was achieved by distortion in Mn-Ga sublattice (Fig. 2(d)). This distortion arose from the shifts of Mn and Ga atoms by about 1 % of atomic coordinates along the x direction. The shift occurred only for atoms at nanotwin boundary (red arrows in Fig. 2(d)) and its direction alternated at each nanotwin boundary. Consequently the internal $(c/a)_{int}$ ratio of tetragonal building blocks of Mn-Ga sublattice decreased from 1.20 to 1.19 (red rectangles in Fig. 1(e)).

Finally, the fully relaxed 4O structure was achieved by alternating shift in Ni sublattice but not only along x direction, but also along y direction and with magnitude less than 0.1 % of atomic coordinates. Although this final relaxation step had negligible effect on the total energy, it resulted in the increase of the internal $(c/a)_{int}$ ratio of

Ni sublattice to 1.21 (black rectangles in Fig. 1(e)). Thus the basic building blocks in Ni and Mn-Ga sublattices are not exactly tetragonal but exhibit very small monoclinic distortion.

Similar stabilizing mechanism as in 4O can be expected also in 10M and 14M structures, since they also contain nanotwin doublelayers. We found the difference of total energies between the geometrically constructed $(3\bar{2})_2^{26}$ and fully relaxed 10M structure which is 2.22 meV/atom; for $(5\bar{2})_2$ and relaxed 14M it is 1.62 meV/atom. In analogy with the 4O structure we suggest that the largest contribution to this energy reduction originates from the shifts of Mn and Ga at the nanotwin boundaries. For fully relaxed 10M structure, these shifts are indicated by red arrows in Fig. 2(f).

The alternating shifts of atomic positions in Mn-Ga sublattice result in significant reduction of the total energy and thus are crucial for stabilization of all structures containing nanotwin doublelayer (4O, 10M and 14M). The shifts of atomic positions also explain why harmonic description of modulation is insufficient for full description of the structure. As consequence of these shifts the Ni and Mn-Ga sublattices in 4O structure exhibit different internal $(c/a)_{int}$ ratio of their corresponding tetragonal building blocks (Fig. 1e). Detailed analysis of interatomic distances indicates different interactions between Ni atoms and Mn/Ga atoms and formation of very strong Ni-Mn and Ni-Ga bonds in the nanotwin boundary plane.

Due to higher symmetry the alternating shifts cannot be realized in NM structure since each atom has the same number of nearest neighbours and the strong bonds cannot be formed. In 10M or 14M structures the shifts and strong bonds can be formed but only in nanotwin boundaries enclosing nanotwin doublelayer, Fig. 1(b)

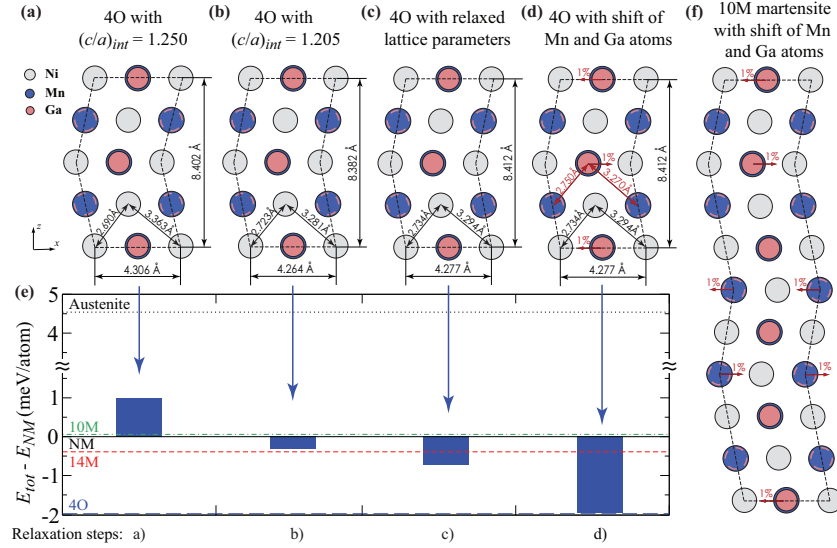


FIG. 2: (Color online) (a-d) Changes in the 4O structure during the relaxation process and (e) corresponding total energies for each structure with respect to the total energy of NM martensite. Total energies of fully relaxed 4O (blue dashed line), 14M (red dashed line), 10M (green dash-and-dotted line) and austenite (black dotted line) are marked. Dashed circles mark Ga atoms in the atomic layer underneath the figure plane. The small red arrows indicate the shift of Mn and Ga atoms in the nanotwin boundaries responsible for the significant total energy decrease. (f) Fully relaxed 10M structure with the shifts of Mn and Ga atoms marked.

and (c)). Only the 4O structure has enough flexibility to allow this distortion in whole lattice which significantly reduce the total energy. For stress-induced 14M \rightarrow NM transformation the direct growth and annihilation of fully formed doublelayers was confirmed by in-situ observation in TEM³⁶.

The energy of modulated 10M and 14M structures, consisting of doublelayers interleaved with NM structure, is similar to the energy of the pure NM structure, Fig. 2(e). This seems to be in contradiction with our statement on the beneficial contribution of doublelayers and associated lattice distortion to the total energy. To get the right interpretation of the observation, one need to consider that the energy of particular structure is the result of competition between positive contribution of nanotwin boundary energy⁴⁶ and negative contribution of boundary-boundary interaction across the doublelayer. In 10M and 14M, the two boundaries enclosing the doublelayer can interact only with each other across the short distance of two atomic planes. In 4O, the number of mutual boundary-boundary interactions per doublelayer is two times larger than that in 10M and 14M. From this reasoning we conclude that the boundary-boundary interaction energy must be negative, and it is immediately seen why the 4O structure is a distinct case with much lower energy than 10M or 14M. However, also other factors as structure symmetry or magnetic interactions have to be taken in the account for full understanding of energy differences between martensitic structures.

The clear evidence for the 4O stability is provided by the calculated DOS displayed in Fig. 3. In contrast with DOS of austenite or NM martensite, the Fermi level,

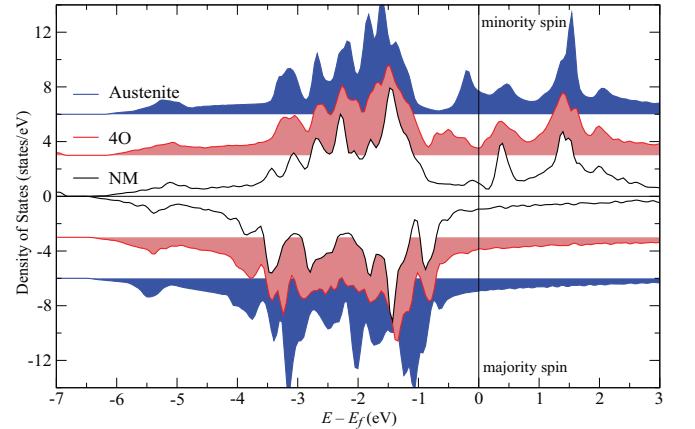


FIG. 3: (Color online) Density of states (DOS) for NM, 4O and austenitic structure. The zero energy corresponds to the Fermi level E_f .

E_f , lies exactly in the middle of a pseudo-gap for minority spin channel, separating bonding and antibonding states. The austenite exhibits the Jahn-Teller peak right below the E_f (blue curves in Fig. 3), which splits due to the tetragonal distortion of NM structure. However, the states at E_f still remain occupied in NM (black curves in Fig. 3). Similar partial occupation at E_f has been reported also for 10M and 14M structures (e.g. Fig. 8 in Ref.³⁰). The lowest occupation at E_f arises uniquely in 4O structure (red curves in Fig. 3). As discussed above, it originates from the strong bond in nanotwin-boundary plane, significantly lowering the total energy.

To get deeper insight into the stability of the 4O structure, we employed Generalized Solid State Nudged Elastic Band (G-SSNEB) method⁴⁷ to find transformation path from austenite to 4O structure. This method allows determining the pathways of solid-solid transformations and energy barriers involving both atomic and unit-cell degrees of freedom with the knowledge of starting and final lattice only. In our case the structures between austenite and 4O martensite were linearly interpolated by ten images and then each image was relaxed with respect to pathway coordinate by G-SSNEB procedure to obtain minimum energy path. We have found a very tiny energy barrier (in order of calculation error) between austenite and 4O. Using the same G-SSNEB procedure to calculate transformation between austenite and NM martensite we obtained the barrier and transformation path corresponding to the tetragonal deformation path already described in literature^{11,12,21,35} confirming the validity of this approach. The barrierless transformation between austenite and 4O is not surprising as austenite, unstable at 0 K, transforms easily to low-symmetry ground state due to the Fermi surface nesting^{11–14} and Jahn-Teller effect^{15–17}.

Question arises why the 4O structure has not yet been reported experimentally in Ni-Mn-Ga. First of all, our calculations were limited only to stoichiometric Ni₂MnGa at 0 K. The stability of 4O will be strongly influenced by temperature, impurities and compositional disorder as these can destabilize nanotwin doublelayers. In the Ni-Mn-Sn alloy⁴⁸, the 4O is destabilized by increasing Mn content, which results in 4O, 10M, 14M and NM sequence⁴⁸. From the point of view of the theory of adaptive martensite²⁵ the 10M or 14M martensites can be seen

as accommodated 4O structure with stacking errors.

In summary, based on *ab initio* calculations we propose stable 4O phase in Ni₂MnGa, which is formed by nanotwin doublelayer stack. The lowest total energy of the 4O phase indicates that the nanotwin doublelayer is the most stable building element of Ni-Mn-Ga modulated martensites and the nanotwinning or modulation is natural property of low-temperature Ni₂MnGa phases. The 4O structure is mainly stabilized by the shifting of Mn and Ga atoms at the nanotwin boundary due to the different types of interactions in Ni and Mn-Ga sublattices. We found that similar shifting exist also in nanotwin boundaries of 10M and 14M structures. Thus the presence of nanotwin doublelayers in modulated martensites reduces considerably the total energy. This explains why stable modulated phases always include the nanotwin doublelayers. Although the 4O structure in Ni-Mn-Ga has not yet been confirmed experimentally, it brings alternative view of martensitic structures which can be relevant even for other nanotwinned materials.

Acknowledgments

This research has been supported by the Ministry of Education, Youth and Sports within the support programme National Sustainability Programme I (Project NETME CENTRE PLUS LO1202) and from the Large Infrastructures for Research, Experimental Development and Innovations project IT4Innovations National Supercomputing Center LM2015070 and by the Czech Science Foundation (Projects No. 14-22490S and No. 16-00043S).

* zeleny@fme.vutbr.cz

¹ K. Ullakko, J. K. Huang, C. Kantner, R. C. OHandley, and V. V. Kokorin, *Appl. Phys. Lett.* **69**, 1966 (1996)

² A. Sozinov, N. Lanska, A. Soroka, and W. Zou, *Appl. Phys. Lett.* **102**, 021902 (2013)

³ M. E. Gruner, P. Entel, I. Opahle, and M. Richter, *J. Mater. Sci.* **43**, 3825 (2008)

⁴ O. Söderberg, Y. Ge, A. Sozinov, S.-P. Hannula, and V. K. Lindroos, in *Handbook of Mag. Mat.*, Vol. 16, edited by K. H. J. Buschow (Elsevier Science, Amsterdam, 2006) pp. 1–39

⁵ O. Heczko, N. Scheerbaum, and O. Gutfleisch, in *Nanoscale Magnetic Materials and Applications*, edited by J. Liu, E. Fullerton, O. Gutfleisch, and D. Sellmyer (Springer Science & Business Media, 2009) pp. 339–439

⁶ M. Acet, L. Mañosa, and A. Planes, in *Handbook of Mag. Mat.*, Vol. 19, edited by K. H. J. Buschow (Elsevier Science, Amsterdam, 2011) pp. 231–289

⁷ V. V. Martynov and V. V. Kokorin, *J. Phys. III France* **2**, 739 (1992)

⁸ N. Lanska, O. Söderberg, A. Sozinov, Y. Ge, K. Ullakko, and V. K. Lindroos, *J. Appl. Phys.* **95**, 8074 (2004)

⁹ A. Çakır *et al.*, *J. Appl. Phys.* **114**, 183912 (2013)

¹⁰ C. P. Opeil *et al.*, *Phys. Rev. Lett.* **100**, 165703 (2008)

¹¹ A. T. Zayak, P. Entel, J. Enkovaara, A. Ayuela, and R. M. Nieminen, *Phys. Rev. B* **68**, 132402 (2003)

¹² P. Entel *et al.*, *J. Phys. D* **39**, 865 (2006)

¹³ C. Bungaro, K. M. Rabe, and A. Dal Corso, *Phys. Rev. B* **68**, 134104 (2003)

¹⁴ A. T. Zayak, W. A. Adeagbo, P. Entel, and K. M. Rabe, *Appl. Phys. Lett.* **88**, 111903 (2006)

¹⁵ S. Fujii, S. Ishida, and S. Asano, *J. Phys. Soc. Japan* **58**, 3657 (1989)

¹⁶ P. J. Brown, A. Y. Bargawi, J. Crangle, K. U. Neuman, and K. R. A. Ziebeck, *J. Phys.: Condens. Matter* **11**, 4715 (1999)

¹⁷ S. Ö. Kart, M. Uludoğan, I. Karaman, and T. Çağın, *Phys. Stat. Solidi A* **205**, 1026 (2008)

¹⁸ A. T. Zayak, P. Entel, J. Enkovaara, A. Ayuela, and R. M. Nieminen, *J. Phys.: Condens. Matter* **15**, 159 (2003)

¹⁹ A. T. Zayak and P. Entel, *Mater. Sci. Eng. A* **378**, 419 (2004)

²⁰ H.-B. Luo, Q.-M. Hu, C.-M. Li, R. Yang, B. Johansson, and L. Vitos, *Phys. Rev. B* **86**, 024427 (2012)

²¹ A. T. Zayak, W. A. Adeagbo, P. Entel, and V. D. Buchelnikov, *Phase Transitions* **78**, 259 (2005)

- ²² L. Straka, A. Sozinov, J. Drahokoupil, V. Kopecký, H. Hänninen, and O. Heczko, *J. Appl. Phys.* **114**, 063504 (2013)
- ²³ O. Heczko, V. Kopecký, A. Sozinov, and L. Straka, *Appl. Phys. Lett.* **103**, 072405 (2013)
- ²⁴ J. Pons, V. A. Chernenko, R. Santamarta, and E. Cesari, *Acta Mater.* **48**, 3027 (2000)
- ²⁵ S. Kaufmann *et al.*, *Phys. Rev. Lett.* **104**, 145702 (2010)
- ²⁶ R. Niemann, and S. Fähler, Submitted to *Phys. Status Solidi*, arXiv: 1611.02535 (2016)
- ²⁷ S. Kaufmann *et al.*, *New J. Phys.* **13**, 053029 (2011)
- ²⁸ A. G. Khachaturyan, S. M. Shapiro, and S. Semenovskaya, *Phys. Rev. B* **43**, 10832 (1991)
- ²⁹ N. Xu *et al.*, *Appl. Phys. Lett.* **100**, 084106 (2012)
- ³⁰ R. Niemann, U. K. Rößler, M. E. Gruner, L. Schultz, and S. Fähler, *Adv. Eng. Mater.* **14**, 562 (2012)
- ³¹ B. Dutta, A. Çakr, C. Giacobbe, A. Al-Zubi, T. Hickel, M. Acet, and J. Neugebauer, *Phys. Rev. Lett.* **116**, 025503 (2016)
- ³² D. Seguí, V. A. Chernenko, J. Pons, E. Cesari, V. Khovailo, and T. Takagi, *Acta Mater.* **53**, 111 (2005)
- ³³ L. Straka, O. Heczko, and N. Lanska, *IEEE Trans. Mag.* **38**, 2835 (2002)
- ³⁴ R. Pond, B. Muntifering, and P. Müllner, *Acta Mater.* **60**, 3976 (2012)
- ³⁵ M. Zelený, L. Straka, and A. Sozinov, *MATEC Web of Conferences* **33**, 05006 (2015)
- ³⁶ Y. Ge, N. Zárubová, O. Heczko, and S.-P. Hannula, *Acta Mater.* **90**, 151 (2015)
- ³⁷ M. E. Gruner, habilitation, Universität Duisburg-Essen (2012)
- ³⁸ Y. Sutou, Y. Imano, N. Koeda, T. Omori, R. Kainuma, K. Ishida, and K. Oikawa, *Appl. Phys. Lett.* **85**, 4358 (2004)
- ³⁹ G. Kresse and J. Furthmüller, *Phys. Rev. B* **54**, 11169 (1996)
- ⁴⁰ G. Kresse and J. Furthmüller, *Comput. Mater. Sci.* **6**, 15 (1996)
- ⁴¹ P. E. Blöchl, *Phys. Rev. B* **50**, 17953 (1994)
- ⁴² G. Kresse and D. Joubert, *Phys. Rev. B* **59**, 1758 (1999)
- ⁴³ J. P. Perdew, K. Burke, and M. Ernzerhof, *Phys. Rev. Lett.* **77**, 3865 (1996); **78**, 1396(E) (1997)
- ⁴⁴ M. Methfessel and A. T. Paxton, *Phys. Rev. B* **40**, 3616 (1989)
- ⁴⁵ T. Björkman and O. Grånäs, *Int. J. Quantum Chem.* **111**, 1025 (2011)
- ⁴⁶ M. Gruner, P. Entel, and S. Fähler, in *5th International Conference on Ferromagnetic Shape Memory Alloys ICF-SMA'16, Book of Abstracts*, (Tohoku University, Sendai, 2016) pp. 21–22
- ⁴⁷ D. Sheppard, P. Xiao, W. Chemelewski, D. D. Johnson, and G. Henkelman, *J. Chem. Phys.* **136**, 074103 (2012)
- ⁴⁸ H.-X. Zheng, W. Wang, S. Xue, Q. Zhai, J. Frenzel, and Z. Luo, *Acta Mater.* **61**, 4648 (2013)